Japanese Journal of Applied Physics

The Japan Society of Applied Physics

PROGRESS REVIEW

Calibration and application of Gaussian random field models for exposure and resist stochastic in EUV lithography

To cite this article: Chih-I Wei *et al* 2022 *Jpn. J. Appl. Phys.* **61** SD0806

Japanese Journal of Applied Physics **61**, SD0806 (2022) **PROGRESS REVIEW**
https://doi.org/10.35848/1347-4065/ac54f5

Calibration and application of Gaussian random field models for exposure and resist stochastic in EUV lithography

Chih-I Wei[1*], Azat Latypov[2*], Peter De Bisschop[3], Gurdaman Khaira[4], and Germain Fenger[4]

[1]*Siemens Digital Industries Software, Leuven, Belgium*
[2]*Siemens Digital Industries Software, Fremont, CA, United States of America*
[3]*IMEC, Leuven, Belgium*
[4]*Siemens Digital Industries Software, Wilsonville, OR, United States of America*

[*]E-mail: Chih-I_Wei@mentor.com; Azat_Latypov@mentor.com

Received December 13, 2021; revised February 2, 2022; accepted February 13, 2022; published online May 20, 2022

Gaussian random field (GRF) models for EUV lithography (EUVL) exposure and resist process address the randomness of the EUVL process outcomes manifested as line edge roughness, line width roughness or catastrophic failures of pinching, bridging or missing vias. The paper presents the background of GRF models for EUVL processes and discusses the application of such models for fast calculation of success or failure probability of the lithographic process or various stochastic metrics quantifying the stochastic variability of the EUVL process outcome. The paper further concentrates on the approaches to calibration of GRF models. The presented results demonstrate the accuracy of GRF models by comparing the failure probabilities calculated using fast methods against the same probabilities estimated using Monte Carlo trials. The approaches to calibration of GRF EUVL models are demonstrated on experimentally measured data for one of the EUVL processes implemented at IMEC, Belgium.

1. Introduction

1.1. Motivation and purpose

The resist patterns defining the geometries of the vias, metal interconnects and transistors in modern integrated circuits form as a result of photochemical processes occurring in the resist film during the exposure, post exposure bake and development steps of optical or EUV lithography. For such patterns of more advanced lithographic nodes, especially the ones formed by EUV lithographic processes, each feature forms as a result of a limited number of photochemical reactions between the randomly placed molecular components of the photoresist, triggered by EUV photons absorbed at random locations. Continuing shrinkage of characteristic dimensions of integrated circuit features leads to the stronger dependence of the lithography process outcome on a progressively smaller number of such stochastic photo-chemical events shaping each of these features,[1–3] manifesting itself as line edge roughness, CD non-uniformity or catastrophic failures of pinching or bridging between the lithographic features. Predicting and mitigating the magnitude of the random stochastic fluctuations in the outcome of the EUVL resist exposure and processing is one of the challenges of EUV lithography.[1–3]

This paper proceeds by describing one stochastic model of EUVL exposure and resist process leading to a Gaussian random field (GRF) deprotection. We will briefly explain, referencing the previously published work,[4,5] how such model can be used to efficiently predict the failure probabilities of EUVL process, as well as to calculate the *stochastic metrics*, the quantities quantifying the stochastic variability of the EUVL process, for instance, *pixNOK*[2,3] or *num_Microbridges*[2,3] or others. We will also present examples showing the EUVL process failure probabilities calculated and compared against the same probabilities estimated from brute force Monte Carlo simulations.

Following that, the paper will concentrate on the methods presently used to calibrate the parameters of the GRF stochastic model, based on experimental measurements, for instance the calibration methods using line edge roughness (LER) or line width roughness (LWR) or the methods using the stochastic contours of 2D features.

1.2. Stochastic model for EUV exposure-resist process

One approach[4,5] to modeling and efficiently quantifying the random stochastic fluctuations is based on the fact that, under certain reasonable assumptions, the deprotection in the stochastic model of the exposure and resist process is a GRF, when viewed in a certain simulation region, or a Gaussian random process, when viewed along a certain line or a curve, e.g. along a metrology gauge.

Such approach is based on a consideration[1,6] of the fact that the coordinates $\mathbf{x}_i^{(h\nu)}$ of the absorption point of each EUV photon (e.g. the ith photon out of a total of $N_{h\nu}$ absorbed photons) in the simulation volume of the resist, V, form a random variable (a random vector) with a probability density function given by

$$f^{(h\nu)}(\mathbf{x}) = \beta\, \alpha(\mathbf{x})\, I(\mathbf{x}), \tag{1.1}$$

where $\beta = \left(\int_V \alpha(\mathbf{x})\, I(\mathbf{x})\, d\mathbf{x}\right)^{-1}$ is a normalization coefficient, $\alpha(\mathbf{x})$ is absorbance coefficient of the resist material (usually assumed to be constant and cancelling in (1.1)), and $I(\mathbf{x})$ is the EUV image intensity in resist. The latter image intensity is the square of amplitude of electromagnetic field, a deterministic, "non-random," function, as usually simulated by optical imaging models, accounting for partially coherent illumination, photomask diffraction, diffraction-limited image formation by projection optics, and also the reflection, refraction and light absorption in the wafer film stack (including the resist film).

One may proceed further using a simplified resist process model,[1,6] operating in terms of the deprotection function, $n(\mathbf{x})$. Such deprotection function may represents, e.g. a concentration of the species affecting the removal of the resist material during the development step of the process. In the simplified resist model[1,6] under consideration, the deprotection from the above single ith photon is given by

$$n_i(\mathbf{x}) = G(\mathbf{x} - \mathbf{x}_i^{(h\nu)}), \qquad (1.2)$$

where the averaged result of the complex resist process resulting from this EUV photon is modeled by a single deprotection kernel, G, leading to the total deprotection from $N_{h\nu}$ absorbed photons:

$$n(\mathbf{x}) = \sum_{i=1}^{N_{h\nu}} n_i(\mathbf{x}) = \sum_{i=1}^{N_{h\nu}} G(\mathbf{x} - \mathbf{x}_i^{(h\nu)}). \qquad (1.3)$$

In this simplified resist model,[1,6] given a scalar model parameter t, *the deprotection threshold*, the development step of the resist process results in the removal of the resist material at all points in the simulation volume V, where $n(\mathbf{x}) > t$. At the points where $n(\mathbf{x}) < t$, the resist is retained, and the points where $n(\mathbf{x}) = t$ form the edges of the developed features in the resist.

The exact physical nature of the deprotection function, $n(\mathbf{x})$, and the threshold parameter, t, may be dependent on the type of the photoresist (e.g. chemically amplified photoresist (CAR), metal-oxide photoresist (MOx), or other type of a photoresist) and also the underlying rigorous or empirical model of this resist exposure, processing and development. For models of many types of photoresists, the deprotection function can be thought of as a spatially-varying concentration of certain species defining the removal or the retention of the surrounding infinitesimal volume during the development. For CAR resists, such species are the activated (reacted with acids) deprotection functional groups on the polymer chains. For MOx resists, they are ligands of the metal nano-particles, reacted with the photoelectrons or secondary electrons during the exposure. On the other hand, in empirical OPC resist models and in the cases when the underlying rigorous model of the resist process includes the development model, the deprotection function may be an abstract mathematical level-set function, immediately lacking any physical interpretation or physical units of measurements and serving, along with the threshold value, t, to define the edges, interiors and exteriors of the resist features formed by exposure, processing and development of the photoresist film. In the current work, to cover various possible physical and chemical mechanisms employed in existing and future photoresists, we view the deprotection function as the latter abstract mathematical level-set function, resulting from a deprotection kernel, $G(\mathbf{x})$, with the latter determined in a calibration procedure, based on the experimental measurements of exposed and developed resist patterns, as described and illustrated in Sects. 2.1, 2.2, 3.1 and 3.2 below.

Application of multidimensional Central Limit Theorem and using the statistical laws of total expectation and total covariance to account for the randomness of the number, $N_{h\nu}$, of EUV photons absorbed in the simulation volume, as detailed in Ref. 4, leads to total deprotection, $n(\mathbf{x})$, being a GRF[7] with its mean function, $\mu(\mathbf{x})$, and its covariance function, $C(\mathbf{x}_1, \mathbf{x}_2)$, given by[4]

$$\mu(\mathbf{x}) = \mathrm{E}(n(\mathbf{x})) = \beta\overline{N_{h\nu}} \int_V G(\mathbf{x} - \mathbf{x}')\, \alpha(\mathbf{x}')\, I(\mathbf{x}')\, d\mathbf{x}', \qquad (1.4)$$

$$\begin{aligned} C(\mathbf{x}_1, \mathbf{x}_2) &= \mathrm{Cov}(n(\mathbf{x}_1), n(\mathbf{x}_2)) \\ &= \beta\overline{N_{h\nu}} \int_V G(\mathbf{x}_1 - \mathbf{x}')\, G(\mathbf{x}_2 - \mathbf{x}')\, \alpha(\mathbf{x}')\, I(\mathbf{x}')\, d\mathbf{x}', \end{aligned} \qquad (1.5)$$

where $\mathrm{E}(\cdot)$ and $\mathrm{Cov}(\cdot,\cdot)$ denote, respectively, the statistical operators of expectation (i.e. mean or average) and covariance, $\overline{N_{h\nu}} = E(N_{h\nu})$ is the average number of photons absorbed in V,[8] for the given exposure dose and the given image in resist, $I(\mathbf{x})$.

One can see from (1.4) that the mean function $\mu(\mathbf{x})$ of the deprotection GRF $n(\mathbf{x})$ is nothing but the average absorbed photon density convolved with the deprotection kernel, as one would expect. The covariance function, $C(\mathbf{x}_1, \mathbf{x}_2)$ given by (1.5) provides, for $\mathbf{x}_1 \neq \mathbf{x}_2$, a quantification of statistical dependence between the stochastic fluctuations of $n(\mathbf{x})$ at two given different points in V. For $\mathbf{x}_1 = \mathbf{x}_2$, $C(\mathbf{x}_1, \mathbf{x}_1)$ is a value of variance of stochastic fluctuations of $n(\mathbf{x})$ at the point $\mathbf{x}_1$.

The mean function, $\mu(\mathbf{x})$, and the covariance function, $C(\mathbf{x}_1, \mathbf{x}_2)$, completely define the deprotection GRF, $n(\mathbf{x})$, and the statistics of its spatial variation inside the simulation volume V, including the statistics of various geometrical shapes formed by applying the deprotection threshold t to the deprotection $n(\mathbf{x})$, that is the statistics of the shapes of the features formed in resist as a result of the EUV lithography process. This fact allows to apply many methods[7] developed by statisticians for calculating of statistical properties of such shapes to the practical tasks of calculation of line edge roughness (LER), line width roughness (LWR), *pixNOK*, *num_Microbridges*, pinching or bridging probabilities and many other stochastic metrics or probabilities of interest to lithographers. The description of some of such methods, applicable to practical tasks considered in this paper, can be found in Sect. 3.3. More extensive discussion of such methods and more examples can be found in Refs. 4 and 5.

In many practical applications, we use a discretization of the GRF, $n(\mathbf{x})$, by considering its values sampled at a certain number, M, of pre-specified *sampling points*, $\mathbf{x}_1, \ldots, \mathbf{x}_M$. Such sampling points, for instance, may be the centers of pixels positioned along the metrology gauge, along which we are interested to measure the result of the lithography process, e.g. a CD of a certain feature. It follows from the above considerations that the random vector $\mathbf{n} = [n(\mathbf{x}_1),\ldots,n(\mathbf{x}_M)]^T$ formed from the values of deprotection sampled at the above sampling points, is distributed accordingly to a multivariate normal (MVN) distribution

$$\mathbf{n} \sim \mathrm{N}(\boldsymbol{\mu}, \boldsymbol{\Sigma}), \qquad (1.6)$$

where the entries of the parameters of this MVN distribution, the mean vector, $\boldsymbol{\mu}$, of length M and the M-by-M symmetric positive semi-definite covariance matrix, $\boldsymbol{\Sigma}$, are given by $\boldsymbol{\mu}_i = \mu(\mathbf{x}_i)$ and $\boldsymbol{\Sigma}_{ij} = C(\mathbf{x}_i, \mathbf{x}_j)$.

While the presented derivation uses a simplified resist model (1.2)–(1.3), more general EUV stochastic models accounting for chemical stochastic or species depletion (non-linearity) during the exposure and post-exposure bake as well as contributions to EUVL stochastics from the causes other than exposure-resist stochastic, can be derived and used. For instance, Ref. 5 presents a generalization of the above derivation to account for a depletion of reacting species during exposure and resist process. The same Ref. 5 also discusses and demonstrates one approach for accounting for defocus and delta dose process parameters random variations, in addition to the exposure-resist stochastic.

The background of the stochastic model presented in this section applies to the treatment of the resist film as a 3D volume. Such model can be used to both simulate the 3D phenomena in the resist film and to calculate the probabilities of essentially 3D outcomes of the resist process of interest to an EUV lithographer—for instance, the probability of the given via to fully develop across the resist film, resulting in an opening extending from the top surface of the resist film to the substrate. However, in many practical applications dealing with "full chip" layouts, following the established practice of OPC and OPC verification, a faster 2D version of this stochastic model, based on the averaging of the resist process outcome across the resist film, may be preferable. It can be demonstrated by a direct calculation, that the mean and covariance for the deprotection GRF in such a 2D model can be calculated using the same formulae (1.4) and (1.5) as in the 3D case, with the 3D deprotection kernel replaced with its 2D version, obtained from the 3D deprotection kernel by its averaging across the resist film.

2. Experimental methods

In Sects. 2.1 and 2.2 below we review some of the practiced methods to calibrate the stochastic model described in the previous sections using the experimentally measured scanning electron microscope (SEM) images of certain calibration patterns exhibiting the effects of the exposure-resist stochastic. Section 2.3 below describes the ways the calibrated stochastic model may be used for practical purposes, concentrating on computation of success or failure probabilities and stochastic metrics.

2.1. Method for calibration of GRF stochastic model based on experimentally measured line edge roughness or line width roughness of lines and spaces patterns

The calibration of the stochastic model is preceded by the standard procedure of OPC model calibration, which typically includes a calibration of non-stochastic optical and resist models based on SEM-measured mean (average) dimensions (CDs) of a variety of calibration patterns.

Following the OPC model calibration, the stochastic model is calibrated. Some parameters of the stochastic model can be straightforwardly calculated from the given values of the EUV lithography process parameters. For instance, assuming that the resist absorbance coefficient is constant, $\alpha(\mathbf{x}) = \alpha_0$, it is convenient to introduce the stochastic model parameter called *resist efficiency* as the product $\alpha_0 h$, where h is the thickness of the resist film. The value of resist efficiency can be straightforwardly calculated from the known thickness of the resist film and the extinction coefficient of the resist material, using the Beer–Lambert's law, as illustrated in Sect. 3.1 below. When the stochastic model (1.4)–(1.5) is applied to a certain 3D simulation volume or a 2D simulation area, another parameter that needs be calculated from the given values of the EUV process parameters is the average number of photons, $\overline{N_{h\nu}}$, absorbed during the exposure. This parameter can be straighforwardly calculated[8] given the EUV exposure dose (a known parameter of the EUV process), the image intensity in resist, $I(\mathbf{x})$, and the above resist absorbance, α_0.

In the current approach to calibration, the deprotection kernel, $G(\mathbf{x})$, of the resist model is assumed to be a Gaussian function, parameterized by a single scalar parameter, a standard deviation, which we call *a diffusion length* of the deprotection kernel.

It should be kept in mind, that the diffusion length of the deprotection kernel, introduced this way, parameterizes the combined diffusion effect in the resist process due to all diffusion mechanisms present, accounting for the spread of the deprotection from an absorbed photon with respect to the site of its absorption. Such parameter should not be confused with *acid* diffusion length frequently used as one essential parameter of DUV or EUV CAR processes. The *acid* diffusion length in DUV CARs is usually studied and used since it parameterizes the principal diffusion mechanism in the DUV CARs process—the diffusion (as well as deprotection and quenching reactions) of acids during the post exposure bake (PEB) step of the process. In other families of the resists, the physical mechanism of propagation of the deprotection from the site of photon's absorption may not involve acids at all (MOx resists), or it may involve the propagation mechanisms additional to the acid diffusion (photoelectron and secondary electron propagation through the resist during exposure in addition to the acid diffusion during PEB in EUV CARs).

One current approach to the calibration of this latter parameter is based on exposing and patterning a certain family of lines and spaces patterns and experimentally measuring 3-sigma standard deviations of the lines or spaces CDs (line width roughness, LWR) or 3-sigma standard deviations of the straight edge positions (line edge roughness, LER). Following that, the diffusion length parameter of the deprotection kernel is selected to optimally match the experimentally measured LWR or LER values to the simulated LWR or LER values, for the set of calibration patterns. Such optimization requires the use of the stochastic model described in Sect. 1.2 to calculate the simulated LER or LWR values for each of the calibration patterns and each value of diffusion length parameter tested in the optimization procedure. The methods that can be used to calculate LER or LWR using the stochastic model are described in Sect. 2.3 below. One example of such calibration procedure is detailed in Sect. 3.1 below.

2.2. Method for calibration of GRF stochastic model based on experimentally measured contours of scanning electronic microscopy images

A more generic way to calibrate the stochastic model on the more complex 2D patterns (e.g. via arrays) is based on using SEM measurements to obtain the multiple 2D contours, representing multiple instances of the edges of the same feature, by measuring and processing the SEM images from multiple instances of the same feature patterned at different locations on the wafer. Figure 1(a) shows the contours extracted from a single SEM image, manifesting the roughness of these 2D edges. Such 2D contours are then aligned and overlapped over a single instance of the feature (a unit-cell position), as illustrated in Fig. 1(b), at the top. To extract the stochastic variation "bands" from the overlapped contours, the average contour is calculated from the multiple SEM contours of the feature. Following that, for each cross section, normal to the average contour, the standard deviations (sigmas) of the edge position are calculated from the cross sections of the SEM contours. Following that, the borders of the +/−3 sigma variation stochastic bands are defined by stepping by 3 sigma, respectively, outward and inward from the average contour, in the direction of its

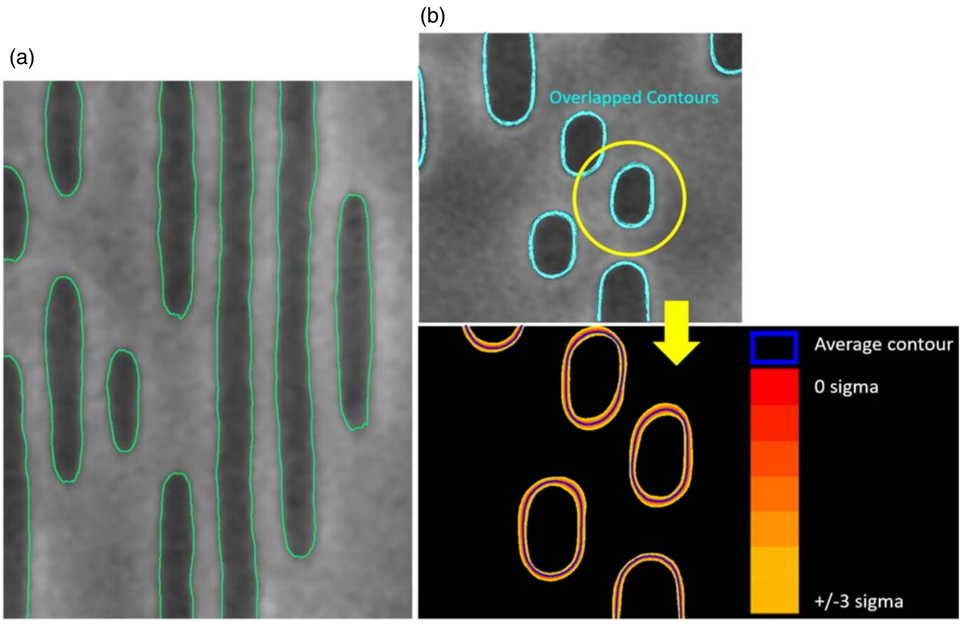

Fig. 1. (Color online) (a) An example of the contours in green which are extracted from one top-down SEM image. (b) A heat map of overlapped contours from average to +/−3 sigma variation. The stochastic +/−3 sigma band is calculated by finding the standard deviation (sigma) at each contour's crossection and plotting the stochastic band boundaries at +/−3 sigma distances from the average contour.

normal. This way, the +/−3 sigma variation stochastic bands are calculated, as the bands bounded by +3 sigma and −3 sigma contours interpolated from the experimentally measured contours [Fig. 1(b), bottom].

The stochastic model calibration procedure then proceeds, similarly to the procedure described in Sect. 2.1, by using the physical exposure dose value known from the process parameters and by calculating the resist efficiency from the known thickness of the resist film and the value of the EUV light extinction coefficient of the resist material (the imaginary component of the resist material complex refraction coefficient). Following these calculations, the diffusion length parameter of the deprotection kernel, $G(\mathbf{x})$, is calibrated by matching the *areas* of the +/−3 sigma variation stochastic bands calculated for multiple features from the experimental data to the areas of the same stochastic bands simulated using the stochastic models, parameterized by the calibrated parameter, the diffusion length. The current approach to a calculation of the simulated +/−3 sigma variation stochastic bands is based on using the fact that the standard deviation of deprotection at any point $\mathbf{x}$ in the resist is $(C(\mathbf{x}, \mathbf{x}))^{1/2}$, where $C(\mathbf{x}_1, \mathbf{x}_2)$ given by (1.5) is a covariance function of the GRF deprotection. The outer and inner boundaries of the simulated +/−3 sigma variation stochastic bands are then approximated by the contours of the fields $\mu(\mathbf{x}) \pm 3(C(\mathbf{x}, \mathbf{x}))^{1/2}$ corresponding to the value of the stochastic model threshold, t.

One example of such calibration procedure is presented in more detail in Sect. 3.2.

2.3. Methods for calculation of failure probabilities and stochastic metrics

After the calibrated GRF deprotection model is available, a lithographer may use it in several possible ways. In one example, on which this paper will concentrate, a lithographer may be interested in deploying the GRF deprotection model to quantify in a reasonably fast simulation the effects of exposure-resist stochastic in order to verify that the given mask layout of the layer, the illumination mode and other process parameters will satisfy the specifications allowed for exposure-resist stochastic effects. Another, more ambitious example may be the use of the stochastic model in an automated exposure-resist stochastic aware optimization algorithm to select the mask layout, the illumination mode and other process parameters to minimize the undesirable exposure-resist stochastic effects. Yet another potential example of application of the GRF deprotection stochastic model is the use of its analytical form (1.4)–(1.5) or some of the analytical results[4,5] stemming from it to gain understanding of the trends driving the stochastic effects to aid the human decision making about the selection of the lithographic process parameters mitigating the undesirable effects of exposure-resist stochastics.

In this section, we will review several options to calculate the failure probabilities and stochastic metrics, with the emphasis on a calculation of gauge-based failure probabilities further illustrated in examples presented in Sect. 3.3.

The calculation of *failure probability* requires a definition of what exactly *the failure* is, in terms of the deprotection function. One generic approach to such a definition was proposed in Ref. 4, based on the observation that the purpose of the traditional optical or EUV lithography can be described as removal of certain pre-defined volumes of the resist film (*integrity sets*, N), while retaining its other pre-defined volumes (*isolation sets, S*).[4] For instance, for a typical metal layer process, the areas in the resist film where the resist is removed will be transformed into metal wires in the subsequent steps of the process, while the areas where the resist is retained will transform into the isolation between these wires. Accordingly, one can define the *integrity sets*, N, as the interiors of the target polygons obtained from the target polygons by application of a certain small negative bias to them. The *isolation sets*, S, can be defined as the exteriors of the polygons formed by application of a certain small positive bias to the target polygons. The probabilities of success, $P_{success}$, and failure, $P_{failure}$, can then be defined in terms of the deprotection function as follows:[4]

$$P_{success} = \Pr\{(n(\mathbf{x}) \geqslant t,\ \text{for all } \mathbf{x} \in N) \text{ and } (n(\mathbf{x}) \leqslant t,\ \text{for all } \mathbf{x} \in S)\}, \quad (1.7)$$

$$P_{failure} = 1 - P_{success}. \quad (1.8)$$

Another family of methods to define success or failure is based on considerations of the outcome of the lithographic resist process along a certain gauge, placed at the critical location of interest by the user or an automated algorithm. For instance, if the gauge is placed across a line feature or a tip-to-tip gap, with a target width equal to CD, such success definition may require that the positions of both edges sampled by this gauge are within a $+/-\Delta CD$ tolerance from their target positions, leading to the success probability defined as:

$$P_{success} = \Pr\{(n(x) \geqslant t,\quad |x| \leqslant 0.5\,(CD - \Delta CD)) \text{ and } (n(x) \leqslant t,\quad |x| \geqslant 0.5\,(CD + \Delta CD))\}, \quad (1.9)$$

where x is the coordinate varying along the gauge, and $x = 0$ corresponds to the center of the line feature or the center of the tip-to-tip gap.

Similarly, if the gauge is placed across the likely bridging or pinching locations, the probabilities of pinching or bridging at this gauge can be defined as

$$P_{bridging} = \Pr(n(x) \leqslant t,\quad \text{for all } x \text{ at the gauge}), \quad (1.10)$$

or, respectively,

$$P_{pinching} = \Pr(n(x) \geqslant t,\quad \text{for all } x \text{ at the gauge}). \quad (1.11)$$

In computational algorithms, one may consider a discretization of the deprotection function by sampling its values at the centers of the regular pixel grid or the pixels spaced along the metrology gauge, resulting in a random vector $\mathbf{n}$ distributed accordingly to a multivariate normal (MVN) distribution (1.6). Calculation of a success or failure probabilities like (1.7)–(1.11) above then reduces to a calculation of a probability that certain components of this random vector are simultaneously above or below the threshold value, t. Such probability, in turn, can be shown to be equal to a certain value of a cumulative distribution function (CDF) associated with a certain MVN distribution. Calculation of the value of CDF for a given MVN is a well-studied problem in statistics, for which many efficient algorithms have been designed and implemented.[9,10]

Along with the calculation of *probabilities* of successes or failures, the lithographers have been traditionally interested in calculation of other quantifications of the stochastic-caused variability, that can be referred to as *stochastic metrics*. For instance, line edge roughness (LER), line width roughness (LWR) and local CD (non)uniformity (LCDU) are traditionally used for this purpose. While the values of LER, LWR and LCDU are dominated by the effects of small and modest deviations of the measured characteristic (e.g. an edge position or a CD of a feature) from their average values, a new family of stochastic metrics has been introduced[2,3] to quantify the likelihood of large, "catastrophic," deviations from the mean measured values, including bridging or pinching between the lithographic features. This family includes "number of defects," *num_Microbridges*, *NOK* or *pixNOK* metrics introduced[2,3] and used to quantify the likelihood of disappearing vias or bridging trenches.[2–4]

One important practical consideration for methods to calculate failure probabilities or stochastic metrics defined above is the computational cost of their calculation. In the following we will review three approaches to calculation of success/failure probabilities or stochastic metrics in the framework of the stochastic model described in Sect. 1.2: brute Monte Carlo methods, fast methods (FM) and very fast methods (VFM), originally described and illustrated in more detail in Ref. 4.

2.3.1. Brute force Monte Carlo methods. In principle, a sufficiently accurate estimate for failure probability or a stochastic metrics can be obtained from brute force Monte Carlo simulations utilizing the photon absorption statistical model (1.1) combined with the simplified resist model (1.3) to generate the deprotection functions within the entire simulation domain for a sufficiently large number of Monte Carlo trials.[4] As described in Ref. 4, such method requires running a Poisson random number generator for every simulation pixel or voxel to determine the absorbed photon density,[4,8] for the current trial. The absorbed photon density is then convolved with the deprotection kernel, $G(\mathbf{x})$, to obtain the deprotection, $n(\mathbf{x})$, for the current trial. This procedure is then repeated for each necessary trial. Every trial is then post-processed to establish if the event of interest (e.g. pinching or bridging) has happened during it, and the total count of the events is calculated for the large number of trials, to arrive to the estimate of probability of such an event. To calculate some statistical metrics, e.g. LER, LWR, *pixNOK* or *num_Microbridges* , for 1D lines and spaces patterns, instead of running multiple trials, one may simulate a very long line using a single trial with a Poisson random number generator, as described above, and, for instance, use the long meandering edges of such long simulated line to obtain the estimates of LER or LWR necessary for calibration methods described in Sect. 2.1. Generally, although brute force Monte Carlo method can be used for verification of other algorithms, it is expected to be too slow for the practical purpose of evaluating the failure probabilities as small as 1×10^{-6} to 1×10^{-9} at least for the most critical of billions of diverse features present on a typical layer of an integrated circuit.

2.3.2. Fast methods (FM). FM are the methods for a calculation of success/failure probabilities or stochastic metrics that still use Monte Carlo trials but run them only for the pixels or voxels involved in the definition of success or failure or the definition of the stochastic metrics. Running Monte Carlo trials for a smaller set of pixels (compared to all pixels in the simulation domain in case of brute force Monte Carlo methods) allows to achieve considerably faster simulation times compared to brute force Monte Carlo trials. The possibility to limit the computations in trials to only a small subset of pixels follows from noticing that a normal distribution with known mean and covariance can be obtained by linear scaling from the standard normal distribution, i.e. a normal distribution with a mean of zero and a unity variance. For instance, one can easily obtain the samples of the scalar random variable u with a given mean $\bar{u}$ and a variance σ^2, $u \sim \mathrm{N}(\bar{u}, \sigma^2)$, given the samples (e.g. outputs from a standard normal random number generator) of a standard normal scalar random variable, $e \sim \mathrm{N}(0, 1)$, by performing a trivial scaling as $u = \mu + \sigma e$. More generally, and more relevant to the discretization of the GRF deprotection, if $\mathbf{n}$ is a random vector distributed accordingly to MVN distribution (1.6), and $\mathbf{\Sigma} = \mathbf{A}\mathbf{A}^T$, where $\mathbf{A}$ ("a square root matrix of $\mathbf{\Sigma}$") is a square matrix of the same dimensions as the covariance matrix $\mathbf{\Sigma}$, and $\mathbf{e} \sim \mathrm{N}(\mathbf{0}, \mathbf{I})$ is a standard normal vector of the same length as $\mathbf{n}$, then $\mathbf{n} = \boldsymbol{\mu} + \mathbf{Ae}$. The validity of this statement can be verified by noticing that $\boldsymbol{\mu} + \mathbf{Ae}$ follows an MVN distribution and by calculating the expectation vector and the covariance matrix of the vector $\boldsymbol{\mu} + \mathbf{Ae}$ to verify that they are equal to, respectively, $\boldsymbol{\mu}$ and $\mathbf{\Sigma}$. This vector analogue of the obvious scalar case allows one to efficiently run the Monte Carlo trials by calculating the trial values of the deprotection $\mathbf{n}$ only at the pixels essential for the definition of success or failure (e.g. only for the pixels located at a certain metrology gauge),[4] or the pixels involved in the definition of stochastic metrics. Reference 4 documents the results of the *pixNOK* stochastic metrics calculated using one of such FM and compared to the experimental measurements of the same stochastic metrics, demonstrating a good agreement. The paper also presents the failure probability calculation performed using one of FM and compared to the same probability estimated by brute force simulation. More of the latter comparisons are also shown in Sect. 3.3 below.

FM can be used to calculate LER or LWR needed in calibration methods described in Sect. 2.1, e.g. by considering the pixels positioned along the nominal positions of the edge of a line, running FM trials as described above to calculate the deprotection along the nominal position of the edge, and then using the linearized dependence of the edge deviation from the deprotection to obtain the random edge displacement at each pixel.

2.3.3. Very fast methods (VFM). Yet another family of methods for calculation of stochastic metrics are VFM.[4] We use this term to refer to the methods where the calculation of the value of stochastic metrics can be accomplished according to an exact analytical formula or a sufficiently well approximating analytical formula, without any Monte Carlo trials. For instance, the average number of defects occurring along the centerline of the given part of the 1D trench, *num_Microbridges*, can be calculated using exact analytical formula based on Rice's formula.[4] Average printed Area (APA)[5] is the stochastic metric useful for assessing the stochastic sidelobe printability, usually caused by SRAFs. Standard deviation of printed area (stdPA)[5] is the stochastic metric quantifying the stochastic variability of the printed feature, e.g. a via. Both APA and stdPA can be calculated using exact analytical formulae, without a need for Monte Carlo trials.[5] In the framework of a simplified model for electrical performance of a via, the ratio of stdPA and APA for the via is equal to the relative standard deviation of its electric conductivity.[5]

3. Results and discussion

3.1. Results for calibration of GRF stochastic model based on experimentally measured line width roughness of lines and spaces patterns, and the discussion

The IMEC first test case adopted a chemical amplified photoresist (CAR) spin-on along with positive tone development (PTD) lithography process and exposed with NXE3300 EUV scanner with 70 nm thickness Ta-based absorber dark field mask on Mo/Si multilayers mirror. The illumination mode is picked as a 45-degree quasar source. The sampling plan of this stochastic modeling is based on 1D line-space of various pitches (36–80 nm) and feature sizes through different dose-focus combinations. SEM images are measured with the field of view (FoV) 900 nm and 1024 pixels resolution. Therefore, line-width roughness (LWR) data are extracted from in-line Hitachi CG5000 with this specific FoV. The edge detection is set to 60% threshold in Hitachi SEM algorithm to extract the CD from the resist trenches. CDs and LWRs are measured from SEM images which are smoothed by averaging 4-lines scan signals in the image.

We first calibrated a non-stochastic OPC model of the process, using standard methods for this purpose. This non-stochastic model calibration includes sampling the dependency between the pitches and mask linewidths of 1D structures and real measured mean wafer CD values for better compact resist model prediction. An optical and mask 3D model were applied to well describe the scanner optics and mask topography.[11] Also, on top-down mask SEM image, the mask manufacture error was inspected and the 2 nm bias on absorber size is used to mimic the reality. Therefore, the focus-CD curve can be well matched between simulation data and experimental data.

To calibrate the stochastic model, we first calculate the resist efficiency $4\pi\, \kappa\, h/\lambda = 0.2925$, where κ is the extinction coefficient of the chosen photoresist and λ is the EUV exposure wavelength, 13.5 nm. Following that, the optimization algorithm was run to select the value of the diffusion length providing the best fit between the simulated and experimentally measured LWR values. To conservatively estimate the magnitude of the residual error corresponding to the best fit, we quantified the latter by the LWR error range over all lines and spaces patterns used in calibration. Such LWR error range was found to be 1.73 nm at the center process conditions of the calibration dataset. If the wider range of the process conditions (+/−2.5% delta dose and 0, 20, 40 nm defocus) is used to quantify the residual LWR error range the observed error range is 2.18 nm—see Figs. 2(a) and 2(b). Since the considerable improvement of the error range was observed in the process of fitting the diffusion length, we considered these LWR error ranges values to be satisfactory. The resulting fitted diffusion length in this calibrated case is 2.08 nm.

3.2. Results for calibration of GRF stochastic model based on experimentally measured contours of scanning electronic microscopy images, and the discussion

In the IMEC second test case also uses a CAR spin-on with PTD lithography process and exposed with NXE3300 EUV

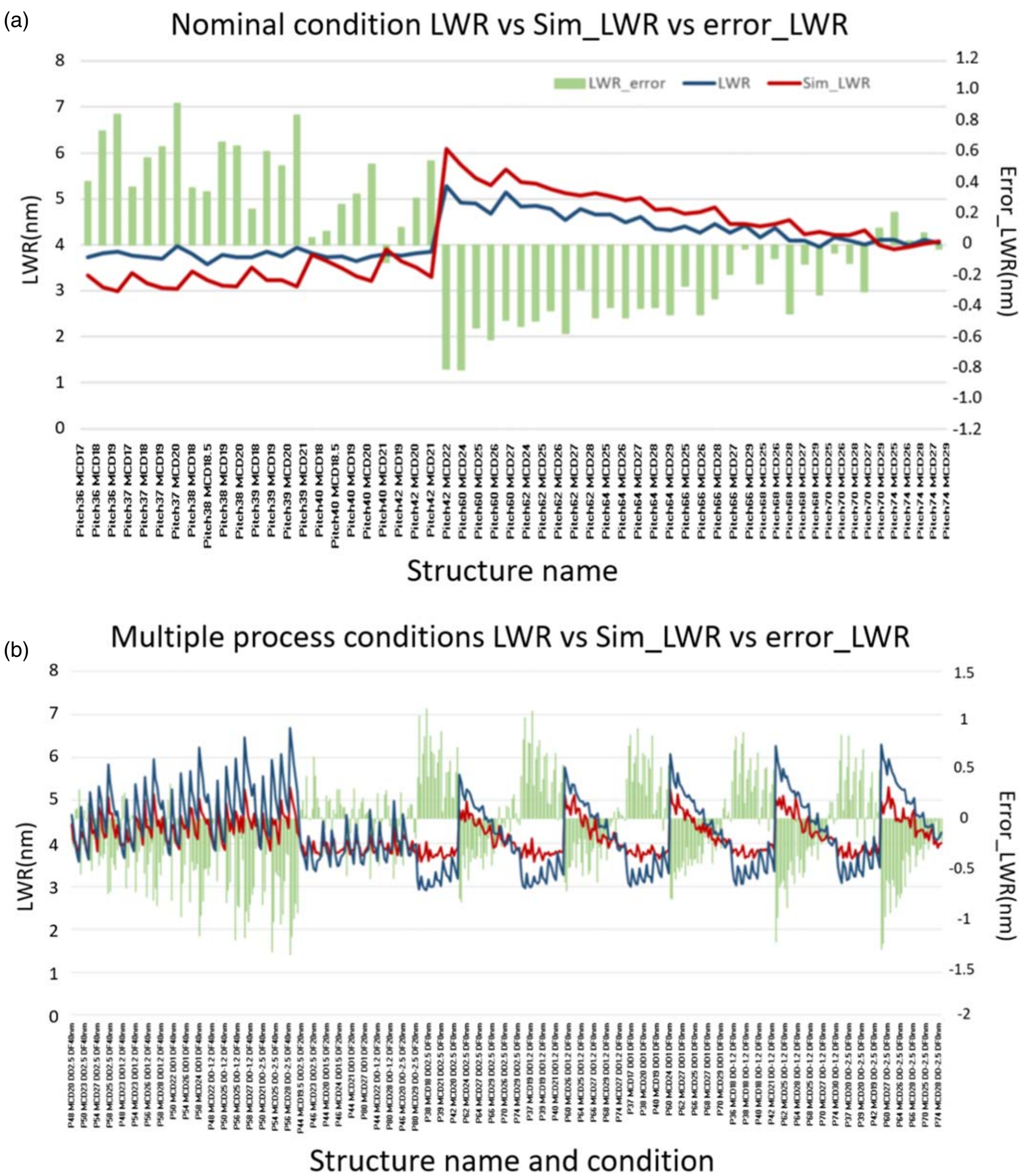

Fig. 2. (Color online) (a) The experimental LWR (LWR), simulated LWR (Sim_LWR) and difference between them (LWR_error) at nominal condition. (b) The fitting data with multiple process window conditions, we considered +/−2.5% delta dose and 0, 20, 40 nm defocus.

scanner with 70 nm thickness Ta-based absorber dark field mask. However, the modeling target designs are 2D shapes which contain finite length of polygons, corner-to-corner, and tip-to-tip environments with the minimum pitch of 46 nm. Furthermore, in experimental metrology tool of this test case, TASMIT NGR3500 Die to Database metrology system is used. The large FoV (LFoV) of 8um*8um with 1 nm pixel size resolution can be set and also post-measurement 2D contours upon the SEM images can be extracted from the same system.[12] The major benefits of introducing LFoV are that the experimental data can be acquired rapidly and also the flexibility to do stochastic modeling in any shape of 2D patterns with local edge deviations of each contour sites. Therefore, it enables users to play around the different weights in between of each site to have better balance in the calibration input data set.

In experimental data, we first extracted experimental 3 sigma variation bands from 25 repetitive sub-cells in one LFoV in this test case. Also, the theoretical resist efficiency in this test case is $4\pi\ \kappa\ h/\lambda = 0.17267$ and the physical dose is 58.6 mJ cm^{-2}. The fitting procedure described in Sect. 2.2, was used to calibrate the diffusion length parameter of the stochastic model. The calculation of the +/−3 sigma variation stochastic bands using the experimental data is based on the 52906 sampling sites around all wafer contours that are in the calibration data set. Furthermore, the verification of through process window conditions (+/−30 nm, +/−60 nm defocus and +/−5% energy latitude) over 205 752 sampling sites were also conducted. The calibrated diffusion length for the stochastic model of the process in this test case was found to be 4.03 nm with good agreement between simulation and experimental 3 sigma variation bands histogram, as illustrated in Figs. 3(a) and 3(b). The Bhattacharyya Coefficient (BC) values illustrated in these figures are calculated according to the formula:

$$BC = \sum_{i=1}^{n} \sqrt{p_i q_i}.$$

This coefficient provides a certain metric of the similarity between two distributions where there are samples of p and q,

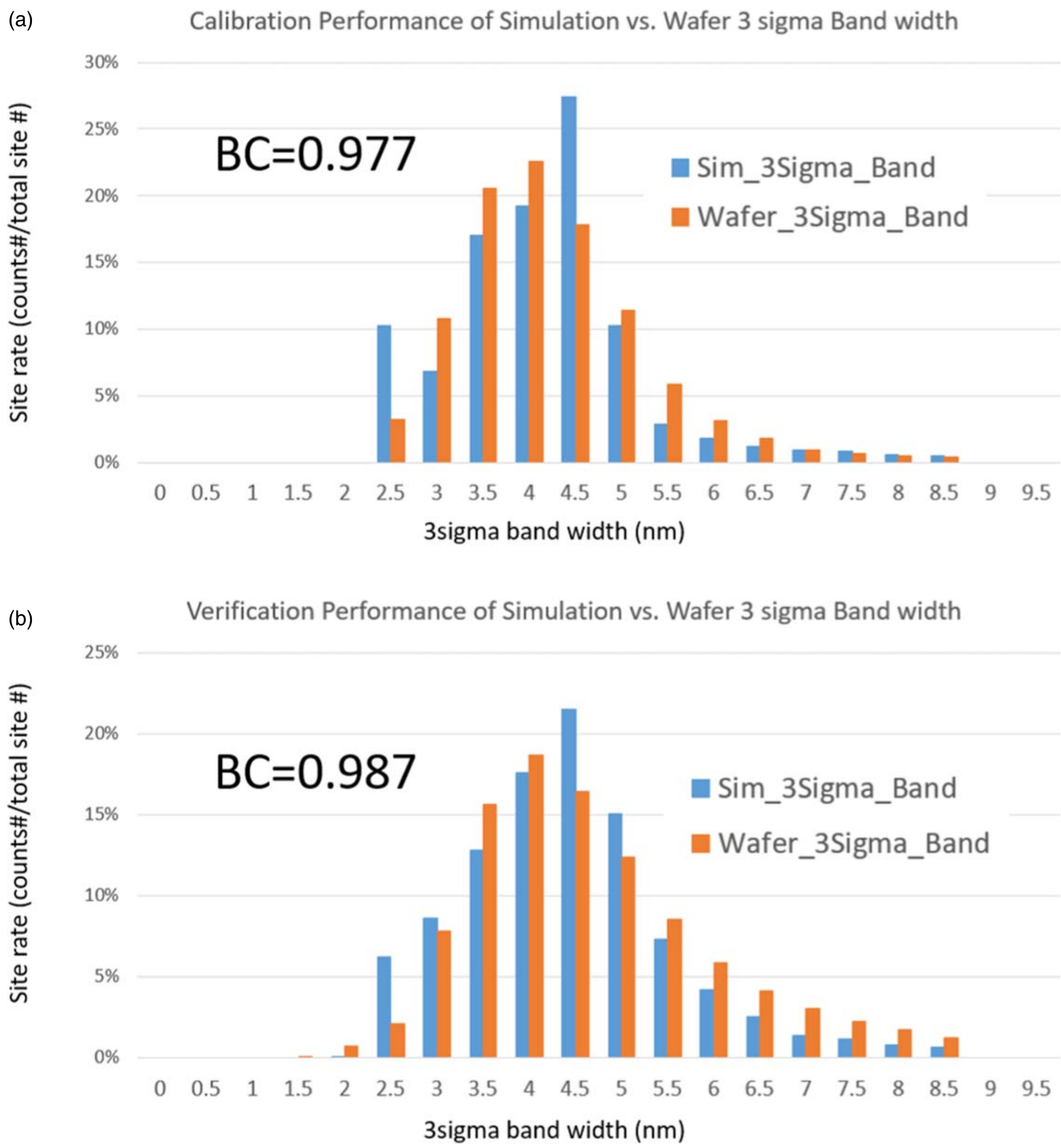

Fig. 3. (Color online) (a) Overlapping histograms of simulated and experimentally measured ("wafer") +/−3 sigma variation stochastic for the calibration data set. (b) The same overlapping histograms for the verification data set. The Bhattacharyya Coefficient (BC) value is calculated as $BC = \sum_{i=1}^{n} \sqrt{p_i q_i}$.

and n is the number of partitions. The $_{pi}$ and q_i are the numbers of sub-group in the ith partition of p and q distributions. To calculate the BC, the interval of those partitions needs to be defined first, and it is set to 0.5 nm in this case.

3.3. Results for calculation of failure probabilities using FM, comparisons against their values estimated from brute force Monte Carlo simulations and the discussion

In this section, we present the results of calculations of failure probabilities for certain representative patterns. These failure probabilities are calculated using two methods. First, we use the FM (as outlined in Sect. 2.3 above) to calculate the appropriate value of MVN cumulative distribution function (MVNCDF). The algorithm described in Ref. 10 is used for this purpose. Second, the same failure probability is estimated by using the brute force Monte Carlo trials, also described in more details in Sect. 2.3 above.

The typical values of the EUV optics imaging parameters ($\lambda = 13.5$ nm for wavelength, NA = 0.33 for numerical aperture of the projection optics and demagnification factor of 4) are used in these simulations. A simplified coherent diffraction-limited imaging model with a Kirchhoff mask model (absorber reflectance of 0.35 (dark areas on the mask) and the multilayer layer reflectance of 0.67 (bright areas on the mask)) is used. Such model does not account for the physical effects of the partially coherent illumination, diffraction on the 3D features of the reflective EUV photomask, reflections and refractions in the wafer film stack. Nevertheless, such simplified imaging model produces the light intensity fields with the spatial frequencies dictated by the resolution of the EUV projection optics, and, when used with representative values of incident dose, this model produces the distributions of the absorbed photons typical for the considered exposure scenarios, as needed for the test cases considered below.

The EUV absorbance coefficient of the photoresist material is assumed to be constant across the 30 nm thick resist film and set to a typical value[8] $\alpha(\mathbf{x}) = \alpha_0 = 4\ \mathrm{um}^{-1}$. The resist model kernel, $G(\mathbf{x})$, is assumed to be a Gaussian function with its standard deviation parameter set to 4.5 nm.

The simulations are performed for the 3 values of the exposure dose, 30 mJ cm^{-2}, 60 mJ cm^{-2} and 90 mJ cm^{-2}. For every value of the dose the threshold of the stochastic resist mode, t, is scaled proportionally to the dose value, thus ensuring that each exposed features prints at the same nominal average dimension for every value of the dose, while the resist-exposure stochastic effects scale appropriately to the dose value.

3.3.1. Gauge CD-based success or failure probability for the gauge placed across the tip-to-tip gap of the lines and spaces pattern. The test case illustrated in Fig. 4 is set up to calculate the probability of the gauge CD based successes or failures. The patterns used are 1:1 lines and spaces array with a tip-to-tip gaps of various width [Fig. 4(a)]. The pitch of these 1:1 lines and spaces patterns is 44 nm. A vertical metrology gauge is placed across one of the tip-to-tip gaps. The one-parametric family of patterns is parameterized by the width of the tip-to-tip gap, measured along this metrology gauge and varying between 10 nm and 42 nm with a step of 4 nm, on the wafer. The probabilities of the gauge CD based success or failures (Sect. 2.3) are calculated for two values of CD tolerance, $\Delta CD = 2$ nm and 4 nm as follows:

$$P_{success} = \Pr\{(n(y) \leqslant t, \ \ |y| \leqslant 0.5\,(CD - \Delta CD)) \text{ and } (n(y) \geqslant t, \ \ |y| \geqslant 0.5\,(CD + \Delta CD))\}, \tag{1.12}$$

$$P_{failure} = 1 - P_{success}, \tag{1.13}$$

as illustrated in Fig. 4(b).

The success probabilities calculated for $\Delta CD = 2$ nm are presented in Fig. 4(c). The low success probabilities resulting from the tolerance parameter $\Delta CD = 2$ nm should not be surprising. This value of the tip-to-tip CD gap tolerance implies that each edge of the gap needs to be confined to the interval (-1 nm; $+1$ nm) for this exposure to be successful,

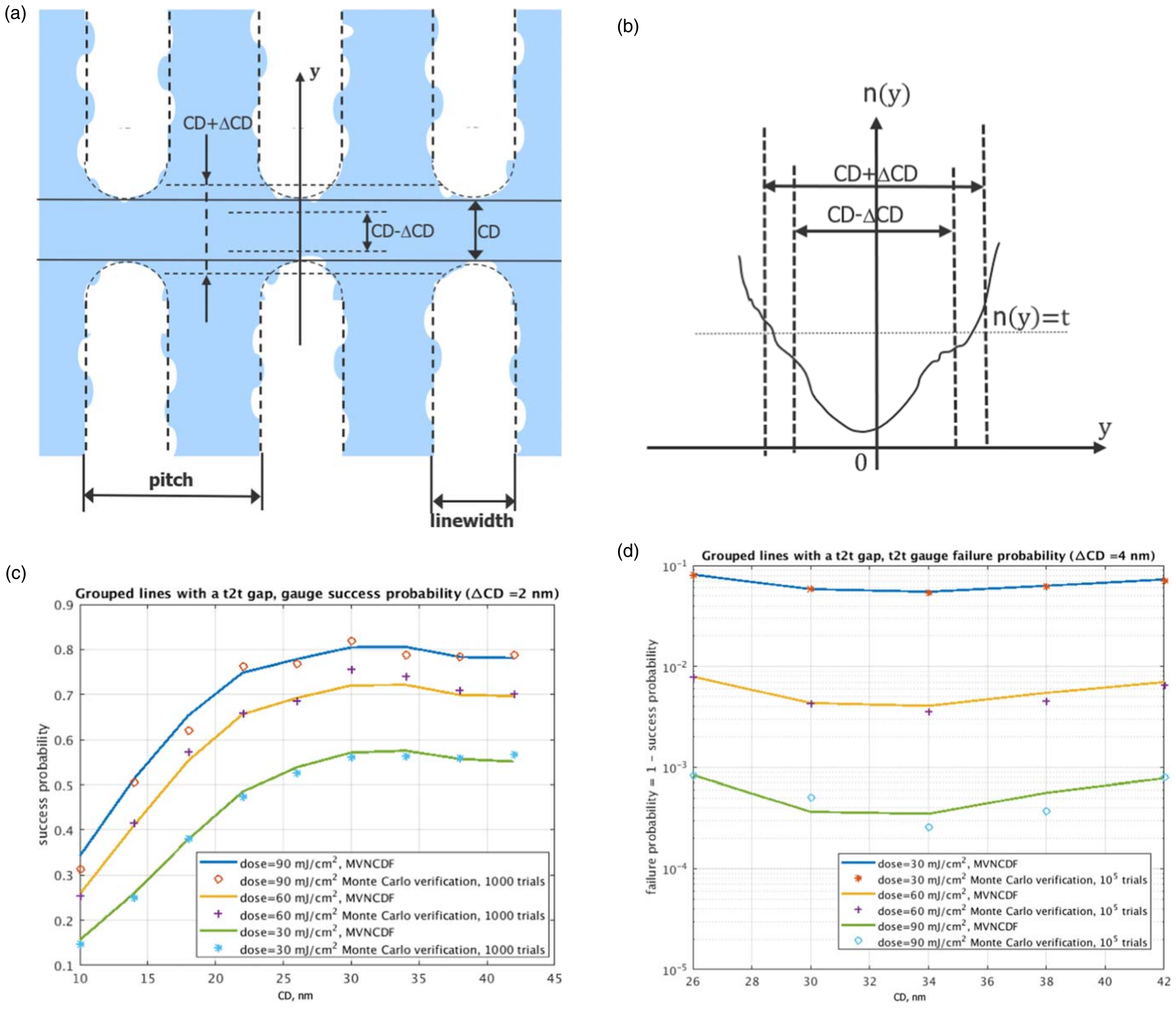

Fig. 4. (Color online) (a) 1:1 lines and spaces array with tip-to-tip gaps, the metrology gauge placed across one of the gaps and the parameters of the gauge CD based success or failure definition; (b) deprotection, $n(y)$, sampled along the tip-to-tip gauge and the illustration of the gauge CD based definitions of success or failure; (c) success probability, as a function of the tip-to-tip gap CD, for tolerance $\Delta CD = 2$ nm, for three values of exposure dose, solid lines—calculated using a fast method (MVNCDF[10]), markers—calculated using brute force Monte Carlo trials (d) failure probability, as a function as a function of the tip-to-tip gap CD, for tolerance $\Delta CD = 4$ nm, for three values of exposure dose, solid lines—calculated using a fast method (MVNCDF[10]), markers—calculated using brute force Monte Carlo trials.

(a)

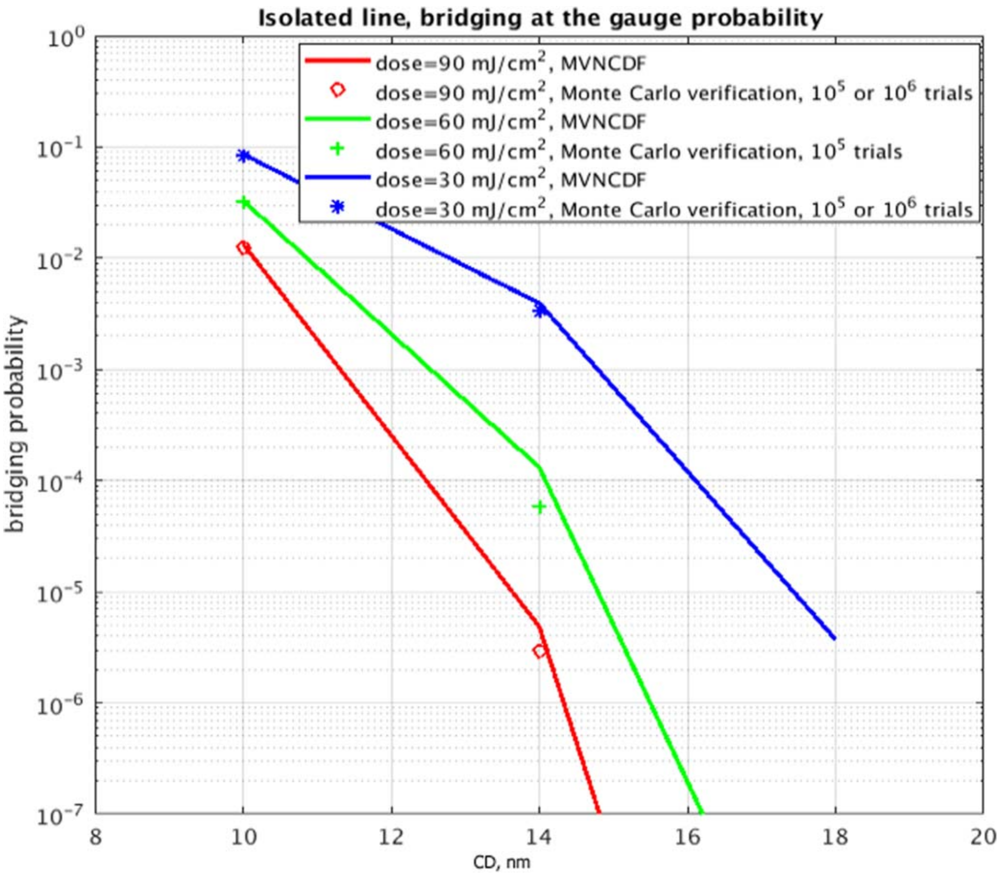

(b)

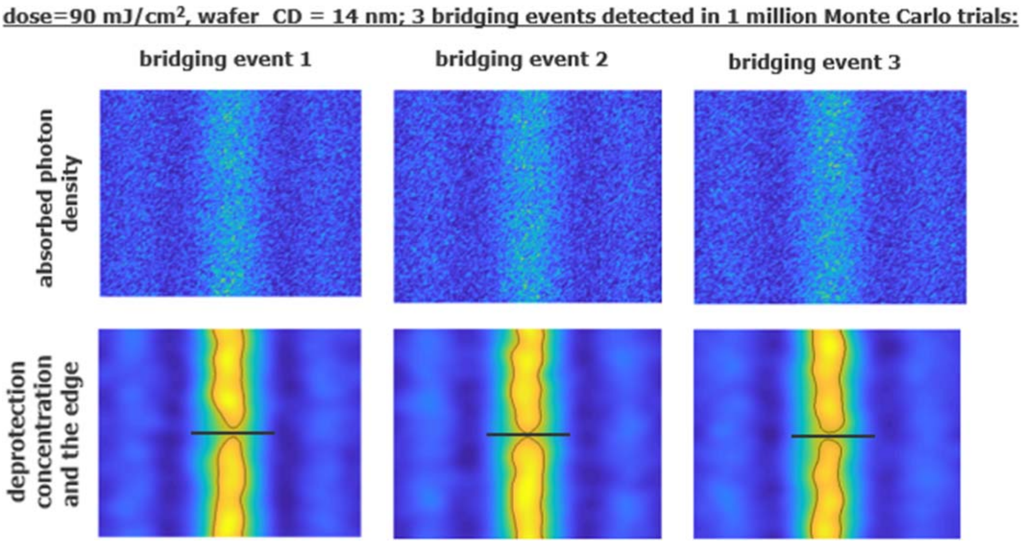

Fig. 5. (Color online) (a) Bridging at the gauge probability, as a function of the trench CD, for the metrology gauge placed across the semi-isolated (pitch = 132 nm) trench at the center of the simulation domain, for the three values of exposure dose, solid lines—calculated using a fast method (MVNCDF[10]), markers—calculated using brute force Monte Carlo trials; (b) dose = 90 mJ cm^{-2}, trench CD = 14 nm, 3 bridging events detected in 1 million Monte Carlo trials.

according to this criterion. For the currently used resist processes, a typical value of one standard deviation of the edge position resulting from the exposure-resist stochastic is about 1 nm. As can be seen from the plot in Fig. 4(c), for the smaller tip-to-tip CD of 10 nm, where the exposure-resist stochastic effects are further amplified by the lower values of the ILS (image log-slope), and for the typical EUV dose of 30 mJ cm^{-2}, the gap CD based success probability for the ΔCD = 2 nm tolerance can be as low as about 15%.

The success probabilities calculated using the FM (the MVNCDF algorithm[10]) shown as solid lines agree well with the same success probabilities estimated using 1000 trials of the brute force Monte Carlo method, shown as markers in Fig. 4(c).

The failure probabilities calculated using the tolerance $\Delta CD = 4$ nm are shown in Fig. 4(d). Besides increasing the value of the tolerance parameter, we calculate the failure probabilities for the range of the gap CD resulting in a more benign image near the gap, resulting in a higher success probabilities (or lower failure probabilities). Again, the failure probabilities calculated using the FM (the MVNCDF algorithm[10]) agree very well with the same probabilities estimated in 10^5 trials of the brute force Monte Carlo method.

3.3.2. Probability of bridging across a trench at the gauge location. In this family of test cases, we consider a family of quasi-isolated trenches patterned in the same simulated EUV process as used in the previous section. This patterning of the family of quasi-isolated trenches is simulated with a pitch of 132 nm, within a 132 nm-by-132 nm simulation domain, with the widths of the trenches varying from 10 nm to 18 nm. We simulated this family of trenches patterned with the same 3 values of EUV doses as in the previous section. These rather narrow trenches were selected in order deal with the higher bridging probabilities that can be verified by a manageable number of Monte Carlo trials.

For each trench width value, the bridging at the gauge probability is defined according to (1.10), and it is calculated using the MVNCDF algorithm[10] and verified using either 10^5 or 10^6 brute force Monte Carlo trials.

The results of these calculations are shown in Fig. 5(a), again demonstrating a good agreement between the bridging probabilities predicted by the FM MVNCDF algorithm[10] and the estimates in the verification brute force Monte Carlo trials.

Figure 5(b) provides a further illustration to these test cases. As can be seen from Fig. 5(a), for the case of a trench width CD = 14 nm and the exposure dose of 90 mJ cm^{-2}, 10^6 (one million) brute force Monte Carlo trials resulted in 3 trials with bridging occurring at the gauge locations. Figure 5(b) shows the details of these 3 trials—the absorbed photon density map and the colormaps of the deprotection, $n(\mathbf{x})$, within the simulation domain, overlapped with the edge (the contour $n(\mathbf{x}) = t$) and the horizontal black line representing the gauge.

3.3.3. Discussion. The results for the test cases presented in Sects. 3.3.1 and 3.3.2 show a good agreement between the probabilities calculated using FM and brute force Monte-Carlo trials, both for probabilities of the gauge CD based success (edge position is within the prescribed range) and for bridging probabilities evaluated using a single gauge.

It should be noted here that this good agreement is demonstrated between two approaches to calculation of probabilities, both utilizing the simplified resist model (1.3). The comparison between the results of these two approaches, by itself, cannot answer the question of whether the stochastic model based on this simplified resist model, is sufficiently accurate. The latter question has been addressed in Ref. 4 where the pixNOK and num_Microbridges stochastic metrics calculated using one of the FM are compared against their values measured experimentally using scanning electronic microscopy and optical metrology, demonstrating a good agreement.

Nevertheless, the good agreement between the FM MVNCDF calculation and the brute force Monte Carlo trials demonstrated in Sects. 3.3.1 and 3.3.2 can be viewed as an assurance that, for the typical EUV exposures as considered above, the number of absorbed photons is sufficient to guarantee a good accuracy of approximation by a normal distribution (1.6), following from the Central Limit Theorem.

The practical importance of the ability to use the approximation by a normal distribution (1.6) is that it allows to apply the FM and the analytical VFM (Sect. 2.3) enabling applications in SMO and full chip OPC and OPC verification. In our experience with the presented examples, the use of the FM improved the runtime of the probability calculation by 100 to 1000 times, compared to the brute force Monte Carlo method.

4. Conclusions

The exposure-resist stochastic model of the EUV lithography process is presented. Application of the Central Limit Theorem to the simple exposure-resist model results in a GRF deprotection stochastic model.

Two approaches to the calibration of such stochastic models are presented. The first approach uses the values of LER or LWR for the family of 1D lines and spaces patterns and ensures the selection of the stochastic model parameters ensuring the best fit of the simulated LER or LWR values to their experimentally measured values.

The 2nd approach uses a family of 2D patterns and ensures the optimal selection of the calibrated parameters ensuring the best fit of the areas of the simulated $+/-3$ sigma variation stochastic bands to the measured areas of the same bands.

Both approaches are illustrated using the measured data from IMEC EUV lithography processes.

The use of the calibrated stochastic models to efficiently calculate the success or failure probabilities of EUVL process or the values of the stochastic metrics characterizing the stochastic variability of the EUVL process, is also discussed. The examples of calculation of the success or failure probabilities using efficient methods and the comparison against the same probabilities calculated using brute force Monte Carlo trials, are presented.

The potential directions of the future work include more advanced and accurate stochastic models and their calibration and the use of the calibrated stochastic models in OPC and SMO algorithms in order to mitigate the effects of exposure-resist stochastics in EUVL.

Acknowledgments

The authors would like to express their gratitude to Dr. Seiji Nagahara, Tokyo Electron Limited, the Japan Applied Physics Society and the Secretariat of the MNC 2021 conference for the invitation to present at the MNC 2021 conference leading to this publication. The authors would like to thank Qijian Wan, WenMing Wu and Ao Chen and for the programing support of experimental stochastic bands extraction. Thanks to Rajiv Sejpal from RIT, and Werner Gillijns, Sayantan Das from IMEC, and Seulki Kang, Yosuke Okamoto, Kotaro Maruyama from TASMIT for supporting the wafer data. This project has received funding from the ECSEL Joint Undertaking (JU) under grant agreement No 783247. The JU receives support from the European Union's Horizon 2020 research and innovation program and Netherlands, Belgium, Germany, France, Austria, United Kingdom, Israel, Switzerland.

1) G. M. Gallatin, "Resist blur and line edge roughness," Proc. SPIE **5754**, 15 (2005).
2) P. De Bisschop, "Stochastic effects in EUV lithography: random, local CD variability, and printing failures," J. Micro/Nanolithogr. MEMS MOEMS **16**, 041013 (2017).
3) P. De Bisschop and E. Hendrickx, "Stochastic printing failures in EUV lithography," Proc. SPIE **10957**, 109570E (2019).

4) A. Latypov, G. Khaira, G. Fenger, J. Sturtevant, C.-I. Wei, and P. D. Bisschop, "Probability prediction of EUV process failure due to resist-exposure stochastic: applications of Gaussian random fields excursions and Rice's formula," Proc. SPIE **11323**, 113230L (2020).
5) A. Latypov, G. Khaira, G. Fenger, S. Wang, M. Chew, and S. Shang, "Gaussian random field EUV stochastic models, their generalizations and lithographically meaningful stochastic metrics," Proc. SPIE **11609**, 1160917 (2021).
6) S. Lee, (2021), Quantum electrodynamical formulation of photochemical acid generation and its implications on optical lithography, arXiv:2101.12598.
7) R. J. Adler and J. E. Taylor, *Random Fields and Geometry, Springer Monographs in Mathematics* (Springer, New York, 2007).
8) J. J. Biafore, M. D. Smith, C. A. Mack, J. W. Thackeray, R. Gronheid, S. A. Robertson, T. Graves, and D. Blankenship, "Statistical simulation of photoresists at EUV and ArF," Proc. SPIE **7273**, 727343 (2009).
9) A. Genz, *Computation of Multivariate Normal and t Probabilities* (Springer, Berlin, 2009).
10) Z. I. Botev, "The normal law under linear restrictions: simulation and estimation via minimax tilting," J. R. Stat. Soc. B **79**, 125 (2016).
11) K. Adam and A. R. Neureuther, "Domain decomposition methods for the rapid electromagnetic simulation of photomask scattering," J. Micro/Nanolithogr. MEMS MOEMS **1**, 3 (2002).
12) C.-I. Wei et al., "Realizing more accurate OPC models by utilizing SEM contours," Proc. SPIE **11325**, 1132524 (2020).

